Absorption saturation of heavy- to light-hole band transitions in *p*-type InSb

R. B. James
Theoretical Division, Sandia National Laboratories, P.O. Box 969, Livermore, California 94550

Y.-C. Chang
Department of Physics, University of Illinois at Urbana-Champaign, 1110 West Green Street, Urbana, Illinois 61801

(Received 17 March 1988)

We present calculations of the intensity dependence of the free-hole absorption coefficient in *p*-type indium antimonide for high-intensity light with a wavelength near 10 μm. The dominant absorption mechanism is direct inter-valence-band transitions, where a hole occupying a state in the heavy-hole band makes a direct transition to a state in the light-hole band. The absorption coefficient due to this mechanism is predicted to decrease with increasing intensity in a manner closely approximated by an inhomogeneously broadened two-level model. Values for the saturation intensity I_S are reported as a function of the photon energy, lattice temperature, and hole density. The dependence of I_S on the hole concentration allows considerable tunability of the saturation behavior, so that for a fixed laser intensity, the degree of absorption saturation can be adjusted by controlling the doping density of the sample. For lightly doped samples at a temperature of 77 K, the free-hole absorption begins to saturate at intensities of less than 10 kW/cm^2, which is between one and two orders of magnitude smaller than the intensities required to saturate the comparable transitions in Ge and GaAs. The calculated results are also important to measurements of the two-photon absorption coefficient K_2 in InSb, and they indicate that much of the transmission data used to obtain a value for K_2 must be reevaluated.

I. INTRODUCTION

In many *p*-type semiconductors, the absorption of light with a wavelength near 10 μm is dominated by direct free-hole transitions between the heavy- and light-hole bands.[1-6] At high light intensities (>1 MW/cm^2), the absorption due to these transitions has been shown to saturate in *p*-type Ge (Refs. 7–11) and GaAs (Refs. 12 and 13). This nonlinear absorption property has found several applications in the control of CO_2 lasers to obtain large peak output powers. For example, the saturation of the inter-valence-band absorption in *p*-type Ge has been exploited to achieve passively mode locked CO_2 laser pulses of subnanosecond duration,[14-16] to achieve isolation of high-power CO_2 oscillator-amplifier systems,[7-8] and to temporally compress far-infrared laser pulses.[7]

In previous work the saturable absorption of *p*-type Ge was described by modeling the valence bands as an ensemble of two-level absorbers whose level populations approach one another at high light intensities.[9] This "two-level" model predicted that the dependence of the absorption coefficient on the light intensity was given by

$$\alpha(I,\omega)=\alpha_0(\omega)[1+I/I_s(\omega)]^{-1/2}\ , \tag{1}$$

where $\alpha_0(\omega)$ is the heavy- to light-hole band absorption coefficient at low intensity, and $I_s(\omega)$ is the saturation intensity. The nonlinear behavior described in Eq. (1) was found to be reasonably well described experimentally, and values of I_s for *p*-type Ge at room temperature were determined to be about 4 MW/cm^2 for 10.6-μm radiation.[7-10] However, attempts to calculate $I_s(\omega)$ for *p*-type Ge as a function of photon energy using the "two-level" model gave results that disagreed with experiment.[17] A theoretical analysis of the saturable absorption was presented later that realistically treated the initial- and final-hole states in the valence-band structure. The theory also predicted an intensity-dependent free-hole absorption cross section that was approximately given by Eq. (1), and the values of $I_s(\omega)$ deduced from the theory were in good agreement with experiment.[18,19] For the work reported in this paper, we modified the calculational approach of Ref. 19, so that it is much more efficient computationally, and we used the modified theory to predict the absorption saturation of far-infrared radiation in *p*-type indium antimonide.

The usefulness of *p*-type indium antimonide as a saturable absorber or fast optical switch in the far-infrared depends on the amount of power required to alter the material from an opaque to a transparent state (i.e., the value of I_s) and the intensity range over which $\alpha(I)/\alpha_0$ can be decreased. The results of the calculations presented in this paper indicate that the predicted value for I_s in *p*-type InSb is much smaller than the measured values for I_s in *p*-type Ge and *p*-type GaAs, which is primarily due to the lower scattering rates for the resonantly coupled hole states in InSb. Because of the considerably smaller value for I_s, InSb may be more promising for some applications requiring far-infrared saturable absorbers, since much less power is required to switch the material from an opaque to a transparent state.

Apart from direct applications of *p*-type InSb as a saturable absorber, our calculated results indicate that saturation of the heavy- to light-hole absorption cross

section has occurred in many experiments used to measure the two-photon absorption coefficient[20–28] and the plasma formation via impact ionization processes in InSb.[29–31] The inclusion of our theoretical results for $\alpha(I)$ in the model equations of Refs. 27 and 28 causes a large change in the value of the two-photon absorption coefficient at $\lambda=10.6$ μm and a significant modification in the calculated hot-electron distribution functions shown in Ref. 29.

This paper is organized in the following way: In Sec. II the calculational approach is presented; in Secs. III and IV we report the calculated results for the intensity-dependent hole distribution functions and the heavy- to light-hole band absorption cross section, respectively; and in Sec. V we summarize our conclusions. Calculational details are included in the Appendix.

II. THEORETICAL APPROACH

The valence-band structure for small k is determined by degenerate $\mathbf{k}\cdot\mathbf{p}$ perturbation theory using a method developed by Kane[32] based on values of the cyclotron resonance parameters.[33] In Fig. 1, the valence bands of indium antimonide are shown for $\mathbf{k}$ in the [100] direction. There are three bands, each of which is twofold degenerate. The heavy- (h) and light- (l) hole bands are degenerate at $k=0$, and the split-off hole band is separated at $k=0$ by the spin-orbit interaction.

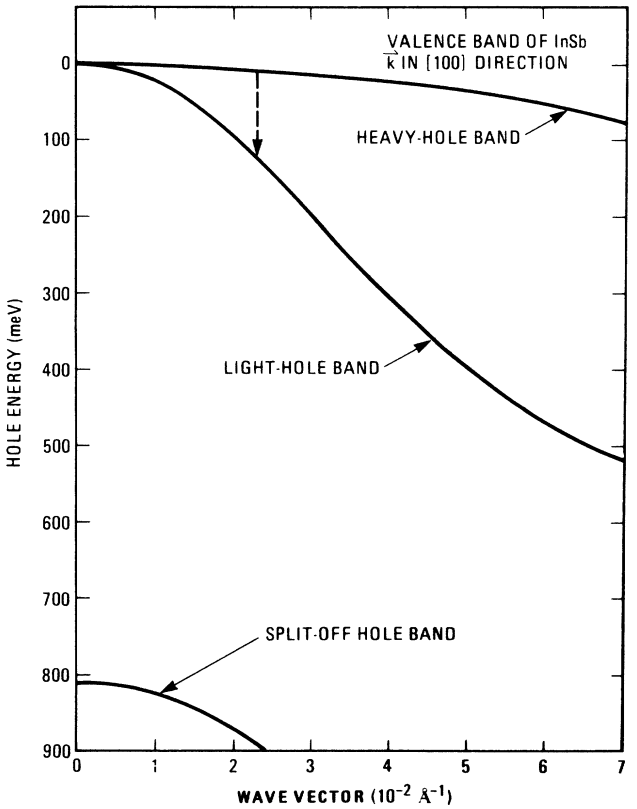

FIG. 1. Valence-band structure of indium antimonide for $\mathbf{k}$ in the [100] direction. Here, an increase in the hole energy corresponds to going vertically downward. The vertical dashed arrow connecting the heavy- and light-hole bands shows the location of the inter-valence-band resonance for light having a wavelength of 10.6 μm.

At $\lambda=10.6$ μm, the direct free-hole absorption cross section in InSb at room temperature is 8.7×10^{-16} cm^{-2}.[34] The intra-valence-band absorption cross section (i.e., phonon-assisted optical transitions) is estimated from Drude-Zener theory to be smaller by 1–2 orders of magnitude. In the calculations presented in this paper, we consider only the direct inter-valence-band transitions between the heavy- and light-hole bands and assume the intra-valence-band absorption to be negligible.

The inter-valence-band absorption coefficient is given by[18,35]

$$\alpha_p(\omega,I)=\frac{4\pi^2e^2}{(K_\infty)^{1/2}m\omega c}\times\sum_{\mathbf{k}}[f_h(\mathbf{k},I)-f_l(\mathbf{k},I)]\,|\,\boldsymbol{\eta}\cdot\mathbf{P}_{hl}(\mathbf{k})\,|^2\times\frac{\hbar\Gamma_{hl}(\mathbf{k})/\pi}{[\hbar\Omega(\mathbf{k})-\hbar\omega]^2+[\hbar\Gamma_{hl}(\mathbf{k})]^2}\ , \tag{2}$$

where the subscripts h (l) designate the heavy- (light-) hole band, K_∞ is the high-frequency dielectric constant, m is the free-electron mass, $\hbar\omega$ is the photon energy, $f_i(\mathbf{k},I)$ is the intensity-dependent probability that a hole state with wave vector $\mathbf{k}$ is occupied in band i, $\mathbf{P}_{bc}(\mathbf{k})$ is the momentum matrix element between Bloch states in bands b and c, $\boldsymbol{\eta}$ is the polarization of the light, $\hbar\Omega$ is the energy difference $[E_h(\mathbf{k})-E_l(\mathbf{k})]$, where $E_i(\mathbf{k})$ is the valence-subband energy for a state with wave vector $\mathbf{k}$ in band i, and $\Gamma_{hl}(\mathbf{k})$ is the average scattering rate for holes in states $(h,\mathbf{k})$ and $(l,\mathbf{k})$.

For all calculated results presented in this paper, we consider the region of temperatures and hole concentrations for which the hole distribution is nondegenerate. The thermal equilibrium energy distribution of the hole carriers for a nondegenerate sample is given by

$$f=(N_h/N_c)\exp(-E/k_BT)\ , \tag{3}$$

where N_h is the density of holes, E is the hole energy, k_B is Boltzmann's constant, and T is the lattice temperature. N_c is the effective density of states defined by

$$N_c=2\left[\frac{m^*k_BT}{2\pi\hbar^2}\right]^{3/2}\ , \tag{4}$$

where m^* is the density-of-states mass.

Since both energy and wave vector are conserved in the optical transitions, only holes in a narrow region of $\mathbf{k}$ space can directly participate in the absorption process. At low light intensities the relaxation mechanisms maintain the hole distribution near its equilibrium value. However, for sufficiently large laser intensities, scattering can no longer maintain the equilibrium distribution, and the occupation probability for resonantly coupled hole states decreases in the heavy-hole band and increases in the light-hole band. Since the absorption is governed by the population difference of these resonant states, this

redistribution leads to a reduced absorption cross section.

In order to calculate the intensity dependence of the absorption coefficient, we must first determine the modification of the distribution functions for holes in the resonant region of the heavy- and light-hole bands. The scattering rate of holes occurs on a picosecond time scale, so for laser pulses of nanosecond or larger duration (the typical experimental situation), transient effects are damped out. We calculate the steady-state hole distribution functions by solving rate equations which include the inter-valence-band optical transitions and the scattering of holes by phonons, ionized impurities, and other free holes.

The derviation of the appropriate rate equations is based on a density matrix formalism and is presented in detail in Ref. 19. The following equations are solved for the distribution functions, $f_h(\mathbf{k})$ and $f_l(\mathbf{k})$, for states in the resonant region of the heavy- and light-hole bands:[19]

$$f_h(\mathbf{k},I)=f_h^e(\mathbf{k})-\frac{\beta(\mathbf{k},I)T_h(\mathbf{k})[f_h^e(\mathbf{k})-f_l^e(k)]}{1+\beta(\mathbf{k},I)[T_h(\mathbf{k})+T_l(\mathbf{k})]}+\frac{F(\mathbf{k},I)T_h(\mathbf{k})+\beta(\mathbf{k},I)T_h(\mathbf{k})T_l(\mathbf{k})[F(\mathbf{k},I)+G(\mathbf{k},I)]}{1+\beta(\mathbf{k},I)[T_h(\mathbf{k})+T_l(\mathbf{k})]} \tag{5}$$

and

$$f_l(\mathbf{k},I)=f_l^e(\mathbf{k})+\frac{\beta(\mathbf{k},I)T_l(\mathbf{k})[f_h^e(\mathbf{k})-f_l^e(\mathbf{k})]}{1+\beta(\mathbf{k},I)[T_h(\mathbf{k})+T_l(\mathbf{k})]}+\frac{G(\mathbf{k},I)T_l(\mathbf{k})+\beta(\mathbf{k},I)T_h(\mathbf{k})T_l(\mathbf{k})[F(\mathbf{k},I)+G(\mathbf{k},I)]}{1+\beta(\mathbf{k},I)[T_h(\mathbf{k})+T_l(\mathbf{k})]} . \tag{6}$$

In Eqs. (5) and (6) we have introduced several auxiliary functions defined by

$$\beta(\mathbf{k},I)=\frac{2\pi^2}{(K_\infty)^{1/2}m^2\omega c}\frac{e^2I}{\hbar\omega}|\boldsymbol{\eta}\cdot\mathbf{P}_{hl}(\mathbf{k})|^2 \times\frac{\hbar\Gamma_{hl}(\mathbf{k})/\pi}{[\hbar\Omega(\mathbf{k})-\hbar\omega]^2+[\hbar\Gamma_{hl}(\mathbf{k})]^2} , \tag{7}$$

$$T_h(\mathbf{k})=\left[\sum_{c,\mathbf{k}'}R_{h\mathbf{k}\to c\mathbf{k}'}\right]^{-1} , \tag{8}$$

$$T_l(\mathbf{k})=\left[\sum_{c,\mathbf{k}'}R_{l\mathbf{k}\to c\mathbf{k}'}\right]^{-1} , \tag{9}$$

$$F(\mathbf{k},I)=\sum_{c,\mathbf{k}'}[R_{c\mathbf{k}'\to h\mathbf{k}}(f_c(\mathbf{k}',I)-f_c^e(\mathbf{k}'))] , \tag{10}$$

and

$$G(\mathbf{k},I)=\sum_{c,\mathbf{k}'}[R_{c\mathbf{k}'\to l\mathbf{k}}(f_c(\mathbf{k}',I)-f_c^e(\mathbf{k}'))] , \tag{11}$$

where f_c^e is the equilibrium value for the distribution function in band c, and $R_{a\mathbf{k}\to b\mathbf{k}'}$ is the rate at which a hole in band a with wave vector $\mathbf{k}$ is scattered into a state in band b with wave vector $\mathbf{k}'$.

The difference in the occupation probabilities, which appears in the expression for the absorption coefficient, is given by

$$f_h(\mathbf{k},I)-f_l(\mathbf{k},I)=\frac{f_h^e(\mathbf{k})-f_l^e(\mathbf{k})}{1+\beta(\mathbf{k},I)[T_h(\mathbf{k})+T_l(\mathbf{k})]}+\frac{T_h(\mathbf{k})F(\mathbf{k},I)-T_l(\mathbf{k})G(\mathbf{k},I)}{1+\beta(\mathbf{k},I)[T_h(\mathbf{k})+T_l(\mathbf{k})]} . \tag{12}$$

The first term in Eq. (12) gives the population difference that would occur for the states at $\mathbf{k}$ if the populations of the states that feed those at $\mathbf{k}$ were given by their equilibrium values. The second term in Eq. (12) accounts for the change in the populations of the states that feed those at $\mathbf{k}$. For those values of $\mathbf{k}$ that are near the resonant region for 10.6-μm radiation, the function $F(\mathbf{k})$ in the second term of Eq. (12) is much larger than $G(\mathbf{k})$. The small value for $G(\mathbf{k})$, compared to $F(\mathbf{k})$, results from the relatively small density of light-hole states, which causes the scattering rate into states in the light-hole band to be much smaller than the scattering rate into states in the heavy-hole band.

The calculation of the intensity-dependent distribution functions requires knowledge of the hole scattering rates [i.e., $T_h(\mathbf{k})$, $T_l(\mathbf{k})$, and $\Gamma_{hl}(\mathbf{k})$]. We first consider the effect of hole-phonon scattering, which is dominant at sufficiently low doping concentrations ($\lesssim 3\times10^{13}$ cm^{-3}). The LO- and TO-phonon dispersion curves of InSb are relatively flat for small $\mathbf{k}$. We assume the hole energy to change by a LO phonon (i.e., 23.7 meV) due to hole–optical-phonon scattering. For the small-$\mathbf{k}$ region near the inter-valence-band resonance, the acoustic phonon energy is quite small, and we neglect it.

The hole-phonon scattering rates are given by the expression

$$R_{a\mathbf{k}\to b\mathbf{k}'}=\frac{2\pi}{\hbar}|M_{\rm op}^{+}|^2\delta(E_a(\mathbf{k})-E_b(\mathbf{k}')+\hbar\omega_0) +\frac{2\pi}{\hbar}|M_{\rm op}^{-}|^2\delta(E_a(\mathbf{k})-E_b(\mathbf{k}')-\hbar\omega_0) +\frac{2\pi}{\hbar}|M_{\rm ac}|^2\delta(E_a(\mathbf{k})-E_b(\mathbf{k}')) . \tag{13}$$

Here, $|M_{\rm op}^{+}|^2$ is the squared matrix element for optical-phonon emission, $|M_{\rm op}^{-}|^2$ is the squared matrix element for optical-phonon absorption, and $|M_{\rm ac}|^2$ is the squared acoustic-phonon matrix element (summed over both emission and absorption processes).

The matrix elements in the hole-phonon scattering rates are calculated on the basis of the deformation potential model.[36,37] The matrix elements are given by

$$|M_{\rm ac}|^2=\frac{E_{\rm ac}^2k_BT}{V\rho u_{\rm l}^2} , \tag{14}$$

$$|M_{\rm op}^{+}|^2=\frac{E_{\rm op}^2\hbar\omega_0}{2V\rho u_1^2}(N_q+1)\ , \tag{15}$$

and

$$|M_{\rm op}^{-}|^2=\frac{E_{\rm op}^2\hbar\omega_0}{2V\rho u_1^2}N_q\ , \tag{16}$$

where ρ is the material density, u_1 is the longitudinal sound velocity, V is the sample volume, $\hbar\omega_0$ is taken to be the LO-phonon energy at the zone center, $E_{\rm ac}$ ($E_{\rm op}$) is the nonpolar acoustical (optical) deformation potential constant, and N_q is the LO-phonon Bose factor defined by

$$N_q=\left[\exp\left[\frac{\hbar\omega_0}{k_BT}\right]-1\right]^{-1}\ . \tag{17}$$

Following Ref. 38 we have neglected angular dependence in the phonon scattering matrix elements and have taken the scattering rates to be the same for the heavy- and light-hole bands. The numerical values for the deformation potential constants appearing in the squared matrix elements are determined by fitting the temperature dependence of the calculated hole mobility to the experimental data.[37–39] The fit to the mobility data gives acoustical and optical deformation potential constants of 2.32 and 4.64 eV, respectively.

For acceptor and hole concentrations greater than about 3×10^{13} cm^{-3}, the scattering of holes by ionized impurities and other free holes becomes important. The ionized-impurity scattering rate for a hole in band i with energy E is given by[40]

$$\Gamma_I^{(i)}=\frac{\pi e^4N_I}{K_0^2(2m_i^*)^{1/2}}\left[\ln(1+\gamma_i^2)-\frac{\gamma_i^2}{1+\gamma_i^2}\right]E^{-3/2}\ , \tag{18}$$

where

$$\gamma_i^2=\frac{2K_0m_i^*k_BT}{\pi N_Ie^2\hbar^2}\ , \tag{19}$$

m_i^* is the free-hole effective mass in band i, K_0 is the low-frequency dielectric constant, and N_I is the concentration of ionized impurities. In the calculation we consider only uncompensated samples of p-type InSb, where the acceptors are all shallow and ionized at 77 K (i.e., $N_I=N_h$).

Following Ref. 41, the rate of hole-hole scattering for a hole in band i with energy E is given by

$$\Gamma_{hh}^{(i)}=\frac{2\sqrt{2}\pi e^4N_h\lambda_i}{K_0^2(m_i^*)^{1/2}}E^{-3/2}\ , \tag{20}$$

where

$$\lambda_i=1+\ln\left[\frac{E}{2\hbar}\left[\frac{K_0m_i^*}{2\pi N_he^2}\right]^{1/2}\right]\ . \tag{21}$$

Using the scattering rates shown in Eqs. (13), (18), and (20), the hole scattering terms $T_h(\mathbf{k})$, $T_l(\mathbf{k})$, and $\Gamma_{hl}(\mathbf{k})$ are computed as a function of the hole energy. We find that the hole-phonon scattering rates increase with increasing energy by approximately $(E)^{1/2}$ and the hole-ionized impurity and hole-hole scattering rates decrease with increasing energy by approximately $(E)^{-3/2}$. The values for $T_h(\mathbf{k})$, $T_l(\mathbf{k})$, and $\beta(\mathbf{k},I)$ are then used to calculate the first term in Eq. (12) for $[f_h(\mathbf{k},I)-f_l(\mathbf{k},I)]$.

The inclusion of the second term in Eq. (12) in the numerical integration of Eq. (2) introduces a correction of between 10% and 25% to the predicted values for the saturation intensity. Since the calculation of the second term in Eq. (12) is somewhat more complicated and its inclusion is relatively unimportant to the calculation of the inter-valence-band absorption saturation, we choose to describe our treatment of this term in the Appendix.

We use Eqs. (A8) and (A9), shown in the Appendix, to obtain approximate values for $F(\mathbf{k},I)$ and $G(\mathbf{k},I)$, which are then used to calculate the second term in Eq. (12) for $[f_h(\mathbf{k},I)-f_l(\mathbf{k},I)]$. The intensity-dependent values for $F(\mathbf{k},I)$ and $G(\mathbf{k},I)$ are also used in Eqs. (5) and (6) to calculate $f_h(\mathbf{k},I)$ and $f_l(\mathbf{k},I)$.

III. INTENSITY DEPENDENCE OF THE HOLE DISTRIBUTION

The functions $\beta(\mathbf{k},I)$, $T_h(\mathbf{k})$, $T_l(\mathbf{k})$, $F(\mathbf{k},I)$, and $G(\mathbf{k},I)$ are computed numerically for states in the resonant region. Figure 2 shows the calculated results for the distribution functions in the heavy- and light-hole bands (multiplied by the effective density of states and divided by the hole concentration) for $\mathbf{k}$ in the [100] and [111] directions and a lattice temperature of 77 K. The solid curves illustrate the thermal equilibrium values for the hole distributions in the heavy- and light-hole bands, and the dashed curves show the modified distribution for states in the resonant region due to excitation by unpolarized light at an intensity of 60 kW/cm^2 and a wavelength of 10.6 μm. The calculation was performed for a free-hole concentration of 5×10^{12} cm^{-3}, in which case the hole-ionized impurity and hole-hole scattering rates are negligible compared to the hole-phonon scattering rate. When hole-ionized impurity and hole-hole scattering mechanisms are small compared to hole-phonon scattering (i.e., $N_h\lesssim3\times10^{13}$ cm^{-3}), the values for the normalized distribution functions, f_h/N_h and f_l/N_h, are independent of the hole density; thus, the normalized distribution functions shown in Fig. 2 are applicable to any hole concentration less than about 3×10^{13} cm^{-3}.

For $\mathbf{k}$ in the [100] direction, the large dip in the occupation probabilities for states in the heavy-hole band and the large increase in the occupation probabilities for states in the light-hole band at $k^2=5.4\times10^{-4}$ Å^{-2} are caused by the direct optical transitions (see Fig. 2). The depletion of the heavy-hole distribution for k^2 in the range of about $(2-5)\times10^{-4}$ Å^{-2} (or E_h in the range of approximately 3–6 meV) is primarily due to the optical bleaching of heavy-hole states in other directions in $\mathbf{k}$ space. This depletion of the resonant heavy-hole states in other $\mathbf{k}$ directions causes a decrease in the scattering of holes into the [100] direction [i.e., a nonzero value for $F(\mathbf{k},I)$]. The non-negligible contribution from $F(\mathbf{k},I)$ in Eq. (5) leads to a decrease in the occupation probabilities for $\mathbf{k}$ in the [100] direction, although the excitation term $\beta(\mathbf{k},I)$ is vanishingly small in this direction for k^2 less

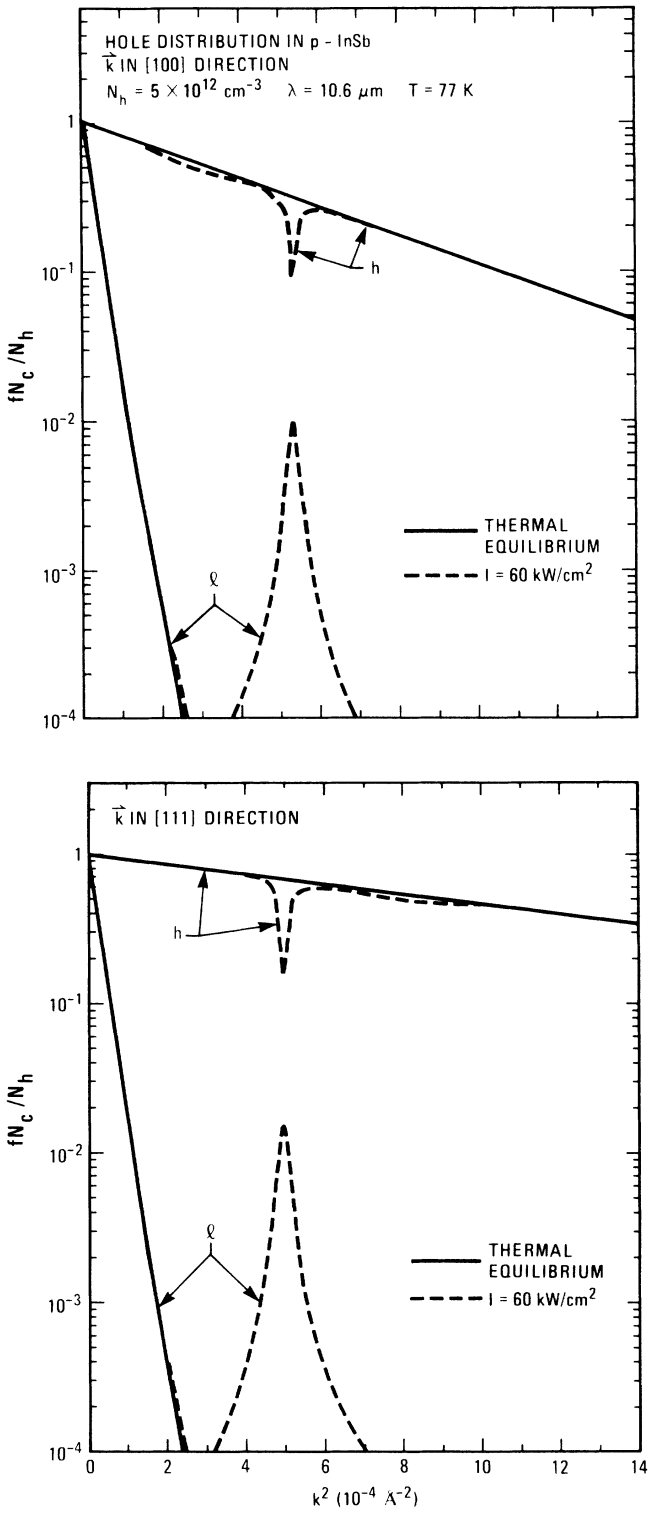

FIG. 2. Calculated hole distribution functions in p-type InSb as a function of k^2 for $\mathbf{k}$ in the [100] and [111] directions. The calculations are performed for a sample with $N_h = 5\times10^{12}$ cm^{-3} and $T=77$ K, and unpolarized light with an intensity of 60 kW/cm^2 and wavelength of 10.6 μm. For comparison, the equilibrium distribution functions are shown by the solid curves. N_c is the effective density of states, and N_h is the hole concentration.

than about 4.5×10^{-4} Å^{-2}.

For $\mathbf{k}$ in the [111] direction, the resonant absorption is peaked at $k^2=5.0\times10^{-4}$ Å^{-2} (see Fig. 2). The small difference in the values of k^2 for which the excitation term $\beta(\mathbf{k},I)$ is peaked in the different $\mathbf{k}$ directions is due to the anisotropy in the valence bands. The depletion of heavy-hole states for k^2 in the range of about $(6-10)\times10^{-4}$ Å^{-2} is due to the contribution from $F(\mathbf{k},I)$ in Eq. (5), which accounts for the intensity-dependent feeding rate of holes into any resonant state $(h,\mathbf{k})$.

At higher hole densities ($\gtrsim 3\times10^{13}$ cm^{-3}), the scattering of holes by ionized impurities and other holes causes an increase in the total scattering rate and introduces a concentration dependence in the calculated values of $(fN_c)/N_h$ for light at a fixed intensity. The result of increasing the hole scattering rate is that higher intensities are required to deplete the population of holes for states in the resonant region, since the photoexcited holes can reroute at a faster rate. Figure 3 shows the values for $(fN_c)/N_h$ for $N_h=5\times10^{15}$ cm^{-3} and $\mathbf{k}$ in the [100] and [111] directions. The solid curves show the thermal equilibrium values at 77 K, and the dashed curves show the distribution for states in the resonant region resulting from excitation at an intensity of 600 kW/cm^2. Comparing Figs. 2 and 3, we note that for higher hole densities (1) larger intensities are required to saturate the resonant transitions, (2) more states are directly involved in the absorption due to the lifetime broadening in the excitation term, and (3) the population of states in the light-hole band contributes a larger amount to the calculated results for $f_h(\mathbf{k},I)-f_l(\mathbf{k},I)$.

The increased role of $f_l(\mathbf{k},I)$ in the saturation behavior of samples with higher hole concentrations results from the energy dependence of the hole scattering rates. Both the hole-impurity and hole-hole scattering rates decrease with increasing hole energy ($\sim E^{-3/2}$ dependence), and the hole-phonon scattering rate increases with increasing energy ($\sim E^{1/2}$ dependence). By increasing N_h from 5×10^{12} to 5×10^{15} cm^{-3}, the total scattering rate for holes in the resonant region of the heavy-hole band is increased greatly by the contribution of hole-ionized impurity and carrier-carrier scattering; the total scattering rate for holes in the resonant region of the light-hole band is increased by a much smaller amount, because the energy of the final-hole state is much larger due to the photon absorption. Thus, for N_h increased to 5×10^{15} cm^{-3}, the heavy-hole lifetime $T_h(\mathbf{k})$ in Eq. (5) for $f_h(\mathbf{k},I)$ is decreased greatly by the hole-ionized impurity and hole-hole scattering terms, and $T_l(\mathbf{k})$ in Eq. (6) for $f_l(\mathbf{k},I)$ is decreased by a much smaller amount due to the smaller contributions from the Γ_I and Γ_{hh} terms. The net result is that at higher hole densities it is relatively more difficult to deplete the resonant states in the heavy-hole band because they are filled at a much higher rate; and for the range of doping concentrations considered, the rate at which the photoexcited holes are emptied out of the resonant light-hole band states is only weakly dependent on N_h.

The dependence of $T_h(\mathbf{k})$ on the hole energy also accounts for much of the anisotropy in the depletion of the hole population for the resonant states in the heavy-hole

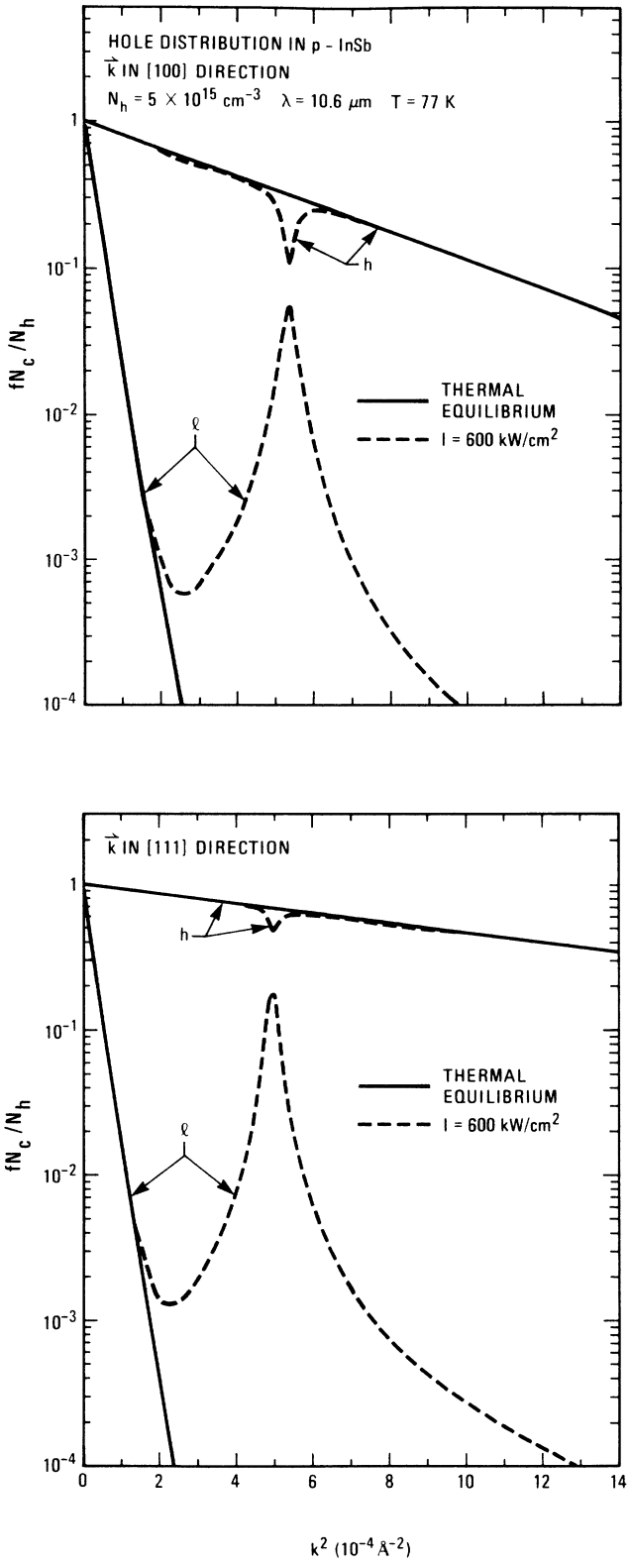

FIG. 3. Calculated hole distribution functions as a function of k^2 for **k** in the [100] and [111] directions. The calculations are performed for a sample with $N_h = 5\times10^{15}$ cm^{-3} and $T=77$ K, and unpolarized light with an intensity of 600 kW/cm^2 and wavelength of 10.6 μm. The equilibrium distribution functions are shown by the solid curves for comparison.

band. For states in the [100] direction, the hole energy is about 7.8 meV at the value of **k** where the excitation term $\beta(\mathbf{k})$ is peaked; for **k** in the [111] direction, the hole energy is about 2.4 meV at the value of **k** where $\beta(\mathbf{k})$ has its maximum value. Thus, for $N_h = 5\times10^{15}$ cm^{-3} and states in the resonant region, the anisotropy in the heavy-hole band causes $T_h(\mathbf{k})$ for **k** in the [100] direction to be significantly larger than the value of $T_h(\mathbf{k})$ for **k** in the [111] direction. For resonant **k** states and unpolarized light, the energy-dependent values for T_h directly affect the calculated results for the heavy-hole distribution [see Eq. (5)], and they are primarily responsible for the degree of anisotropy in the optical bleaching of the resonant states in the heavy-hole band.

The degree of anisotropy in the state filling of the resonant states can be significantly enhanced by using polarized light instead of unpolarized light. For unpolarized light the excitation term $\beta(\mathbf{k},I)$ in Eq. (7) depends strongly on $[E_h(\mathbf{k})-E_l(\mathbf{k})]$; and for a fixed value of $[E_h(\mathbf{k})-E_l(\mathbf{k})]$, it is rather weakly dependent on the specific direction in **k** space. However, for polarized light $\beta(\mathbf{k},I)$ becomes much more dependent on the wave vector, because of the increased **k** dependence in the momentum matrix elements. Figure 4 shows the distribution functions in the heavy- and light-hole bands for $N_h = 5\times10^{12}$ cm^{-3} and light polarized in the [001] direc-

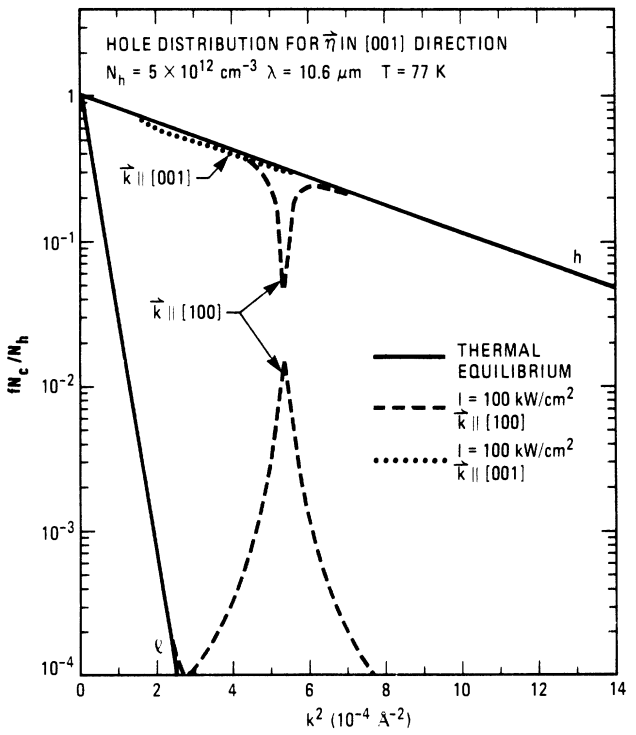

FIG. 4. Calculated hole distribution functions as a function of k^2 for **k** in the [001] and [100] directions. The calculations are performed for a sample with $N_h = 5\times10^{12}$ cm^{-3} and $T=77$ K, and light polarized in the [001] direction with an intensity of 100 kW/cm^2 and a wavelength of 10.6 μm. The solid curves show the thermal equilibrium values, which are equal for the two different directions in **k** space.

tion. The solid curves show the thermal equilibrium values for f_h and f_l at $T=77$ K for $\mathbf{k}$ in the [100] direction. (The equilibrium values are identical for $\mathbf{k}$ in the [100] and [001] directions.) The dashed and dotted curves show the distributions for $\mathbf{k}$ in the [100] and [001] directions due to excitation at an intensity of 100 kW/cm^2. For $\mathbf{k}$ in the [100] direction, the momentum matrix elements in the expression for $\beta(\mathbf{k},I)$ are relatively large compared to the other directions in $\mathbf{k}$ space; and for $\mathbf{k}$ in the [001] direction, the momentum matrix elements in $\beta(\mathbf{k},I)$ are zero, so there is no direct inter-valence-band absorption for $\mathbf{k}$ in this direction. The depletion of the resonant states for $\mathbf{k}$ in the [001] direction results from the reduced elastic scattering of holes from other resonant $\mathbf{k}$ states for which $\beta(\mathbf{k},I)$ is nonzero. The effect of an anisotropic $\beta(\mathbf{k},I)$ is even more evident for resonant states in the light-hole band. For $\mathbf{k}$ in the [100] direction, the resonant light-hole states are pumped directly by the inter-valence-band excitation, and for $\mathbf{k}$ in the [001] direction there is no pumping from the heavy-hole band due to the zero momentum matrix elements. There is some effect on $f_l(\mathbf{k},I)$ from the modified feeding rate [i.e., the nonzero value of $G(\mathbf{k},I)$ in Eq. (6)], but this is quite small because

$$(m_l)^{3/2}/[(m_h)^{3/2}+(m_l)^{3/2}]=5.67\times10^{-3}\ .$$

Physically, this means that for the holes populated in the light-hole band by the inter-valence-band transitions, only 0.6% of these holes are scattered into other light-hole band states and 99.4% are scattered into heavy-hole band states. Thus, the modification of the resonant states in the light-hole band is almost completely determined by the excitation term. Although we find a considerable dependence of $f_h(\mathbf{k},I)$ and $f_l(\mathbf{k},I)$ on the polarization of the incident radiation, the numerical integration of Eq. (2) for $\alpha_p(I)$, which averages the hole distribution over all $\mathbf{k}$ directions, shows only a weak dependence ($<10\%$) of I_s on the direction of the polarization.

Our results for polarized light show that there is considerable anisotropy in the state filling of the resonantly coupled states. If two pulses having orthogonal polarizations are spatially and temporally overlapped on a p-type InSb sample, the polarization of the resultant field will modulate periodically in real space, although the intensity across the sample is uniform. Since the excitation term $\beta(\mathbf{k},I)$ depends strongly on the polarization of the field, the population difference $f_h(\mathbf{k},I)-f_l(\mathbf{k},I)$ will have a preferred orientation that modulates periodically as the pulses propagate through the material. This periodic modulation in space produces an orientational grating similar to that studied by Smirl *et al.*[42] in germanium, and their excite-and-probe techniques can likely be applied to study the state filling of the resonant $\mathbf{k}$ states in the heavy- and light-hole bands of InSb.

IV. INTENSITY DEPENDENCE OF THE INTER-VALENCE-BAND ABSORPTION COEFFICIENT

The intensity-dependent distribution functions are used in the numerical integration of Eq. (2) to calculate the absorption coefficient. The absorption coefficient is computed for intensities between 0 and $10I_s$, and the results are found to be well approximated by the equation

$$\alpha(N_h,\omega,I)=\alpha_0(N_h,\omega)[1+I/I_s(N_h,\omega)]^{-1/2}\ . \qquad (22)$$

This equation differs from Eq. (1) in that there is an explicit dependence of the saturation intensity on the hole density of the sample. This decrease of the absorption coefficient with increasing intensity is the same as one predicts for a system of two-level absorbers that are inhomogeneously broadened.

Figure 5 shows the predicted results (solid curve) for $\alpha_p(I)$ for $N_h=5\times10^{12}$ cm^{-3}, $\lambda=10.6$ μm, and $T=77$ K. The dashed curve in the figure illustrates the results using Eq. (22). The specific value of I_s used in Fig. 5 was determined by fitting Eq. (22) to the numerical results obtained from the integration of Eq. (2) for intensities in the range of 0 to $10I_s$. If only the first term in Eq. (12) is retained [i.e., $F(\mathbf{k},I)$ and $G(\mathbf{k},I)$ are assumed to be 0], the calculated values for $\alpha_p(I)$ have almost exactly the intensity

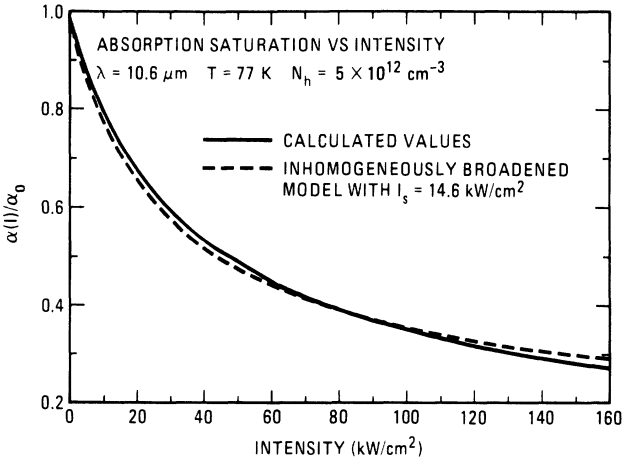

FIG. 5. Calculated absorption coefficient $\alpha(I)$ normalized to its low-intensity value α_0 as a function of intensity. The calculations were performed for $N_h=5\times10^{12}$ cm^{-3}, $T=77$ K, and unpolarized light at a wavelength of 10.6 μm.

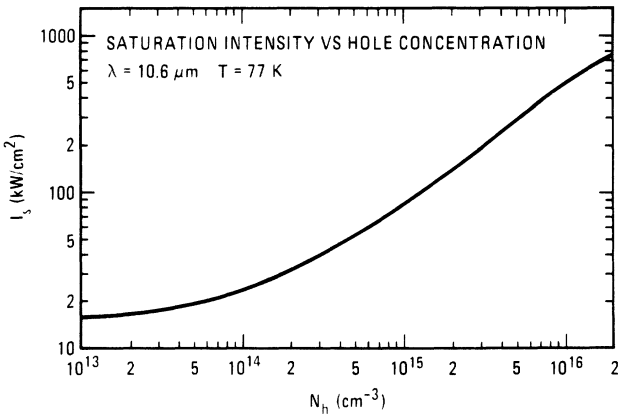

FIG. 6. Calculated saturation intensity I_s as a function of the hole density for p-type InSb at 77 K.

dependence shown by Eq. (22). The second term in Eq. (12), which includes the modified rate of holes being scattered into the resonant region, is smaller than the direct excitation term, and is primarily responsible for the small deviation between Eqs. (2) and (22) as shown in the figure. The numerical results predicted by Eq. (2) could be fit by Eq. (22) to an accuracy of less than 7% for intensities up to 10 times I_s. Although the fit is fairly good, there is a general trend in which the calculated results for $\alpha_p(I)$ decrease a little more rapidly than predicted by Eq. (22), because of the nonzero auxiliary functions $F(\mathbf{k},I)$ and $G(\mathbf{k},I)$ in Eqs. (2) and (12). That is, if we extend the range of intensities used in the fit to higher values, we predict slightly smaller values for I_s. Nevertheless, we choose to fit the calculated results of $\alpha(I)$ for p-type InSb to Eq. (22), because the heavy- to light-hole band saturation behavior of both p-type Ge (Refs. 7–10) and p-type GaAs (Ref. 13) has been shown experimentally to be well described by this equation, and values of $I_s(\omega)$ are available for these materials for purposes of comparison.

The calculated values for I_s are shown in Fig. 6 as a function of the hole density for a lattice temperature of 77 K and unpolarized light at a wavelength of 10.6 μm. We note that I_s is substantially independent of the hole concentration for densities less than about 3×10^{13} cm^{-3}, that is, in the region where the hole-phonon scattering mechanism is dominant. For hole concentrations greater than about 3×10^{13} cm^{-3}, the saturation intensity begins to increase monotonically with increasing hole density due to the increased total scattering rate of the free holes participating in the infrared absorption. For samples in which the scattering of holes in the resonant region of the heavy-hole band is dominated by hole-ionized impurity and hole-hole scattering, we find the saturation intensity to vary approximately linearly with the hole density. This dependence of I_s on the hole density allows considerable tunability of the value of I/I_s be controlling the doping density of the sample; thus, the saturation characteristics can be adjusted in order to be optimal for a specific application.

Since the scattering rates are dependent on the lattice temperature, the saturation behavior also depends on the temperature of the sample. In Fig. 7 we present the results of a calculation of the temperature dependence of I_s in p-type InSb for $N_h=5\times10^{12}$ cm^{-3} and light with a wavelength of 10.6 μm. For this hole density the hole-ionized impurity and carrier-carrier scattering rates are negligible compared to the hole-phonon scattering rate. The computed values for I_s are found to increase monotonically with temperature, because of the increased rate of hole-phonon scattering at the higher temperatures. Since there is a rather strong dependence of I_s on temperature, it is also possible to tune the absorption saturation by controlling the temperature of the p-type InSb sample.

At higher hole concentrations, the temperature dependence of I_s is different due to the effect of hole-ionized impurity and hole-hole scattering terms. Figure 8 shows the values of I_s as a function of T for $N_h=5\times10^{15}$ cm^{-3} and $\lambda=10.6$ μm. The computed results for I_s also increase monotonically with temperature, although the temperature dependence is weaker than the results shown in Fig. 7 for $N_h=5\times10^{12}$ cm^{-3}. In general the values of I_s depend strongly on the temperature because of the hole-phonon scattering terms and strongly on the hole density because of the hole-ionized impurity and carrier-carrier scattering terms.

The dependence of I_s on the wavelength of the laser radiation is shown in Fig. 9 for $T=77$ K and photon energies in the range of 110–140 meV, which is the range of photon energies that can be easily generated with a transversely excited atmospheric (TEA) pressure CO_2 laser. The values of I_s are displayed for two different doping

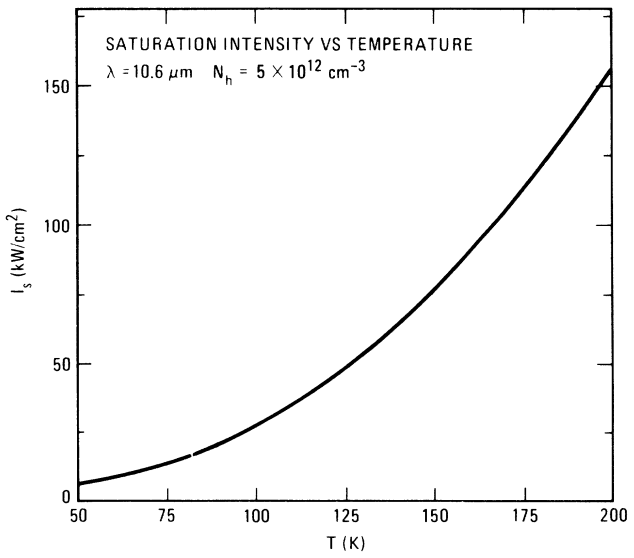

FIG 7. Saturation intensity as a function of the lattice temperature for $N_h=5\times10^{12}$ cm^{-3} and unpolarized light at a wavelength of 10.6 μm.

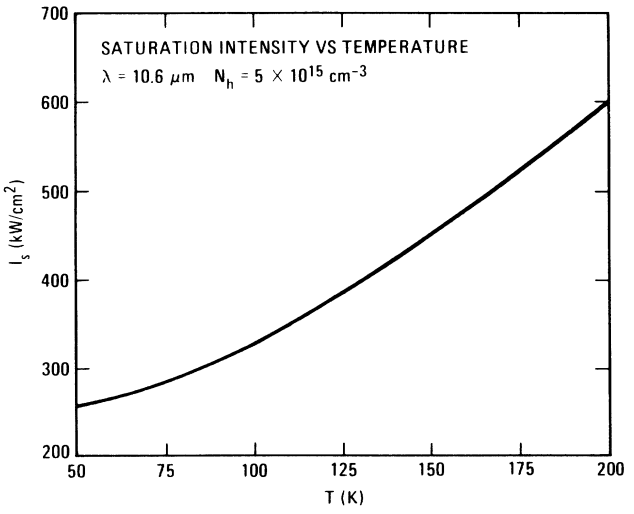

FIG. 8. Saturation intensity as a function of the lattice temperature of $N_h=5\times10^{15}$ cm^{-3} and unpolarized light at a wavelength of 10.6 μm.

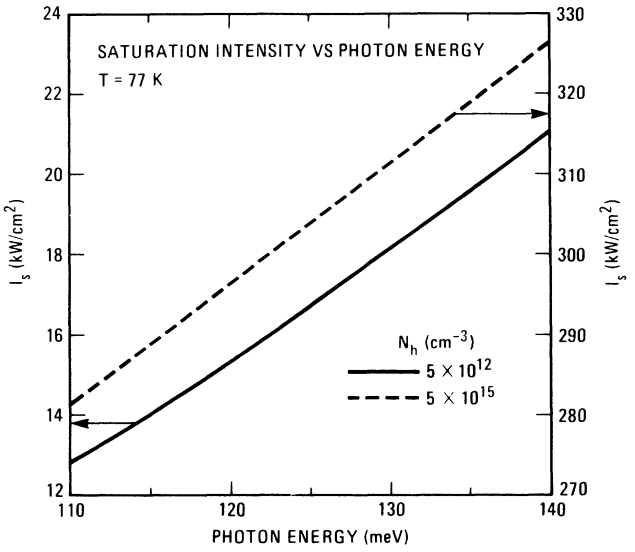

FIG. 9. Saturation intensity as a function of the photon energy for p-type InSb at 77 K. The solid (dashed) curve is for a sample with a hole concentration of 5×10^{12} (5×10^{15}) cm^{-3}.

densities; the solid curve shows I_s for $N_h=5\times10^{12}$ cm^{-3} and the dashed curve shows I_s for $N_h=5\times10^{15}$ cm^{-3}. At both doping densities the saturation intensity increases monotonically with the photon energy, although the wavelength dependence is much stronger at $N_h=5\times10^{12}$ cm^{-3}.

An effect of increasing the photon energy is to move the resonant region of the heavy- and light-hole bands farther away from the zone center (see Fig. 1), which modifies both the scattering and excitation rates of the resonantly coupled states. Thus, for higher photon energies, the inter-valence-band resonance occurs at larger wave vectors, which means larger hole energies in the valence bands. An increase in the hole energies for states in the resonant region causes an increase in the phonon scattering rates and a decrease in the ionized impurity and carrier-carrier scattering rates. The excitation term $\beta(\mathbf{k},I)$ is also modified by the scattering rates, the ω^{-2} factor, and the momentum matrix elements [see Eq. (7)]. The ω^{-2} factor in $\beta(\mathbf{k},I)$ causes the excitation rate to decrease with increasing photon energy, which clearly contributes to an increase in I_s with $\hbar\omega$ for all hole concentrations. The momentum matrix elements tend to increase with increasing $\hbar\omega$, although the contribution from the momentum matrix elements to the values for $I_s(\omega)$ is somewhat less than the contribution from the ω^2 factor in the excitation term.

For both applications and comparison of theory with experiment, it is important that the dynamic range in the saturable absorption be as large as possible. The maximum reduction of the total absorption coefficient is, in general, determined by the value of I/I_s and the onset of the two-photon absorption (TPA) process. The TPA process increases the free-carrier absorption via the generation of nonequilibrium electron-hole pairs. At 77 K and a wavelength of 10.6 μm, the two-photon absorption across the band gap must be considered for intensities greater than several tens of kW/cm^2.[28] Thus, an experimental test of the free-hole absorption saturation should be performed on lightly doped p-type samples that are cooled to about 77 K or less (i.e., the samples should have a relatively small value for I_s), so that a significant reduction in the intervalence-band absorption cross section occurs prior to the onset of two-photon absorption. This condition is satisfied for p-type InSb samples when $[\alpha_p(I=0)-\alpha_p(I)]\gg K_2 I$.

Presently, we have been unable to find experimental data on the transmission of high-intensity CO_2 laser light through lightly doped p-type InSb, although the transmission measurements should be fairly straightforward to perform. There exist several papers reporting measurements of the two-photon absorption process[20–28,43–49] in InSb, but all of these studied were conducted on n-type crystals, instead of p-type crystals. There are two primary reasons than n-type InSb was used to study the TPA of CO_2 laser radiation: (1) The absorption cross section of free electrons is much less than the free-hole cross section, so the change in the total absorption due to two-photon transitions is much larger in n-type samples, and (2) it is much easier to make good ohmic contacts on n-type InSb for samples covering a wide range of electrical conductivity. Even though all of the transmission measurements were performed on n-type samples, it is likely that significant free-hole absorption saturation occurred in many of the measurements, and that the inclusion of our intensity-dependent intervalence-band absorption coefficient greatly modifies the conclusions obtained from these TPA studies. That is, for laser intensities at which nonequilibrium carriers (ΔN) are created in their n-type samples, the absorption associated with the presence of the nonequilibrium free holes is larger than the absorption associated with the two-photon absorption mechanism (i.e., $\Delta N\,\sigma_p I > K_2 I^2$). For example, a value for K_2 of 16 cm MW^{-1} was obtained by Doviak *et al.*[27] using model equations that neglect the inter-valence-band absorption by nonequilibrium free holes altogether, and a value of almost two orders smaller ($K_2=0.2$ cm MW^{-1}) was later obtained from the same data by Gibson *et al.*[28] using equations that assume σ_p to be given by its thermal equilibrium value (i.e., independent of the laser intensity). The inclusion of our theoretical results for $\sigma_p(I)$ in the model equations of Refs. 27 and 28 results in a value for K_2 that is somewhat larger than 0.2 cm MW^{-1} and much closer to the theoretical values of 1.03 cm MW^{-1} by Lee and Fan[26] and 1.1 cm MW^{-1} by Danishevskii *et al.*[22] The degree of importance of the intensity dependence of σ_p in the transmission data of Refs. 20–28 and 43–49 depends on the specific value of I_s and the amount of free-hole absorption, relative to the total absorption coefficient, in the different materials.

V. SUMMARY AND CONCLUSIONS

We have presented calculated results for the absorption saturation of heavy- to light-hole band transitions in p-type InSb. We find that the intensity dependence of the inter-valence-band absorption cross section is closely approximated by an inhomogeneously broadened two-level

model, and values of the saturation intensity are reported as a function of the photon energy, lattice temperature, and hole concentration. For the temperatures and concentration range where hole-phonon scattering dominates hole-impurity and hole-hole scattering, I_s is found to be independent of the hole density. For larger hole concentrations where hole-impurity and carrier-carrier scattering are not negligible, the saturation intensity increases monotonically with increasing hole density. For lightly doped p-type InSb at a temperature of 77 K, we find that the free-hole absorption begins to saturate at intensities of less than 10 kW/cm^2. The theoretical values for the saturation intensity of lightly doped InSb are found to be between 1 and 2 orders of magnitude smaller than the measured values of I_s for p-type Ge and GaAs. Given the interests in saturable absorbers of 10.6-μm radiation, these relatively small values of I_s for p-type InSb may be of significant practical importance.

ACKNOWLEDGMENTS

The authors gratefully acknowledge support from the U.S. Department of Energy. We would also like to thank D. L. Smith, M. I. Baskes, A. J. Antolak, and S. M. Foiles for many useful discussions.

APPENDIX: CALCULATION OF THE FUNCTIONS $F(\mathbf{k},I)$ AND $G(\mathbf{k},I)$

We now describe the calculation of the auxiliary functions $F(\mathbf{k},I)$ and $G(\mathbf{k},I)$. From the definition of these functions and Eqs. (5) and (6), one can write equations which determine $F(\mathbf{k},I)$ and $G(\mathbf{k},I)$ in terms of $f_h(\mathbf{k}',I)$ and $f_l(\mathbf{k}',I)$. Since there is assumed to be no angular dependence in the hole scattering matrix elements, the function $F(\mathbf{k},I)$ depends on the energy $E_h(\mathbf{k})$ and not on the specific direction in $\mathbf{k}$ space; similarly, $G(\mathbf{k},I)$ depends on $E_l(\mathbf{k})$ and not on the wave vector.

For acoustic-phonon and ionized-impurity scattering, the energy of the initial-hole state in the scattering event is essentially the same as that of the final-hole state (i.e., the scattering is approximately elastic). As a result, hole states that can scatter into a resonant optical transition region by acoustic-phonon and ionized-impurity scattering are, for the most part, already in the resonant region. Thus, the population of these states is directly depleted by the inter-valence-band transitions. Assuming that $F(\mathbf{k},I)=0$, therefore, overestimates the feeding rate into the resonant states by elastic scattering processes.

For optical-phonon scattering, the energy of the initial-hole state in the scattering event differs from that of the final-hole state by the optical-phonon energy (i.e., $\sim$23–24 meV). Thus, hole states that scatter into resonant states in the heavy- or light-hole bands by optical-phonon scattering are themselves outside of the resonant region. As a result, the population of these states is not directly depleted by the optical transitions.

The hole-hole scattering term couples a hole state with wave vector $\mathbf{k}$ to all other $\mathbf{k}$ states. Furthermore, the equations for $F(\mathbf{k},I)$ and $G(\mathbf{k},I)$ are no longer linear when carrier-carrier scattering is included. In order only to couple states with other states on the same constant energy surface (elastic scattering) or other constant energy surfaces that differ by the optical-phonon energy, we assume that the rate of scattering into the resonant region by hole-hole collisions is given by its thermal equilibrium value [i.e., there is no direct contribution to $F(\mathbf{k},I)$ and $G(\mathbf{k},I)$ from hole-hole scattering]. This approximation is clearly valid at the lower hole densities, in which case the hole-phonon scattering is dominant, but it begins to break down at higher hole concentrations where the carrier-carrier scattering makes the largest contribution to the equilibrium feeding rate of holes into the resonant region. For the results presented in this paper, the maximum hole density considered is 2×10^{16} cm^{-3}.

By including only the hole-phonon and hole-ionized impurity scattering terms, we can describe the functions $F(\mathbf{k},I)$ and $G(\mathbf{k},I)$ by one-dimensional (rather than three-dimensional) equations. In the calculation, we assume initially that $F(\mathbf{k},I)=G(\mathbf{k},I)=0$, so that Eq. (5) for $f_h(\mathbf{k},I)$ becomes

$$f_h^{(0)}(\mathbf{k},I)=f_h^e(\mathbf{k})-\frac{\beta(\mathbf{k},I)T_h(\mathbf{k})[f_h^e(\mathbf{k})-f_l^e(\mathbf{k})]}{1+\beta(\mathbf{k},I)[T_h(\mathbf{k})+T_l(\mathbf{k})]} \tag{A1}$$

for states in the resonant region of the heavy-hole band. Substituting the zeroth-order approximation of $f_h(\mathbf{k},I)$, shown by Eq. (A1), into the definition of $F(\mathbf{k},I)$ yields

$$F^{(0)}(E_h(\mathbf{k}),I)=\sum_{\mathbf{k}'}R_{h\mathbf{k}'\to h\mathbf{k}}\left[\frac{-\beta(\mathbf{k}',I)T_h(\mathbf{k}')[f_h^e(\mathbf{k}')-f_l^e(\mathbf{k}')]}{1+\beta(\mathbf{k}',I)[T_h(\mathbf{k}')+T_l(\mathbf{k}')]}\right]. \tag{A2}$$

The term in Eq. (10) that describes the modified feeding rate of holes into the resonant region of the heavy-hole band from states in the light-hole band is not included in Eq. (A2), since $\beta(\mathbf{k}',I)$ is negligibly small (nonresonant) for these states in $\mathbf{k}$ space.

For $\mathbf{k}$ in the resonant region, the hole–optical-phonon scattering rates are much smaller than the elastic scattering rates, because (1) optical-phonon emission is not energetically allowed for resonant states in the heavy-hole band, and (2) optical-phonon absorption is weak since the LO-phonon occupation probability (N_q) is much less than unity at a lattice temperature of 77 K. Thus, the primary contribution to $F(\mathbf{k},I)$ is from elastic processes. In addition, $\beta(\mathbf{k}',I)$ in Eq. (A2) is large for elastic scattering processes that scatter from $\mathbf{k}'$ into $\mathbf{k}$, and $\beta(\mathbf{k}',I)$ is small for optical-phonon scattering processes that scatter from $\mathbf{k}'$ to $\mathbf{k}$, since the states with wave vector $\mathbf{k}'$ are nonresonant. Thus, for resonant $\mathbf{k}$ states, we can approximate $F^{(0)}(E_h(\mathbf{k}),I)$ by the expression

$$F^{(0)}(E_h(\mathbf{k}),I)=\sum_{\mathbf{k}'} R^{(\text{elastic})}_{h\mathbf{k}'\to h\mathbf{k}}\left[\frac{-\beta(\mathbf{k}',I)T_h(\mathbf{k}')[f_h^e(\mathbf{k}')-f_l^e(\mathbf{k}')]}{1+\beta(\mathbf{k}',I)[T_h(\mathbf{k}')+T_l(\mathbf{k}')]}\right], \tag{A3}$$

where $R^{(\text{elastic})}_{h\mathbf{k}'\to h\mathbf{k}}$ is the rate of scattering by elastic processes from states in the heavy-hole band with wave vector $\mathbf{k}'$ into states in the same band with wave vector $\mathbf{k}$. Since the scattering rates depend only on the energy of the state and not on the specific direction in $\mathbf{k}$ space, Eq. (A3) can be written as

$$F^{(0)}(E_h(\mathbf{k}),I)=T_h(\mathbf{k})\sum_{\mathbf{k}'} R^{(\text{elastic})}_{h\mathbf{k}'\to h\mathbf{k}}\left[\frac{-\beta(\mathbf{k}',I)[f_h^e(\mathbf{k})-f_l^e(\mathbf{k}')]}{1+\beta(\mathbf{k}',I)[T_h(\mathbf{k})+T_l(\mathbf{k}')]}\right]. \tag{A4}$$

Using the same procedure, we obtain the following expression for the auxiliary function $G^{(0)}(E_l(\mathbf{k}),I)$ for states in the resonant region:

$$G^{(0)}(E_l(\mathbf{k}),I)\cong T_l(\mathbf{k})\sum_{\mathbf{k}'} R^{(\text{elastic})}_{l\mathbf{k}'\to l\mathbf{k}}\left[\frac{\beta(\mathbf{k}',I)[f_h^e(\mathbf{k}')-f_l^e(\mathbf{k})]}{1+\beta(\mathbf{k}',I)[T_h(\mathbf{k}')+T_l(\mathbf{k})]}\right]. \tag{A5}$$

The term in Eq. (11) that describes the feeding rate of holes into the state $(l,\mathbf{k})$ from the heavy-hole band is vanishingly small, since $\beta(\mathbf{k}',I)$ is nonresonant for these states. For a fixed hole energy, the density of states in the heavy-hole band is about 175 times the density of states in the light-hole band; thus,

$$\sum_{\mathbf{k}'} R^{(\text{elastic})}_{l\mathbf{k}'\to l\mathbf{k}} \ll \sum_{\mathbf{k}'} R^{(\text{elastic})}_{h\mathbf{k}'\to h\mathbf{k}}$$

and for all states in the resonant region, $F(E_h(\mathbf{k}),I)\gg G(E_l(\mathbf{k}),I)$.

Substituting the above expression for the auxiliary functions of $F^{(0)}(E_h(\mathbf{k}),I)$ and $G^{(0)}(E_l(\mathbf{k}),I)$ into Eqs. (5) and (6) gives expressions for $f_h^{(1)}(\mathbf{k},I)$ and $f_l^{(1)}(\mathbf{k},I)$ to first order in F and G. Using the first-order expressions for $f_h^{(1)}(\mathbf{k},I)$ and $f_l^{(1)}(\mathbf{k},I)$, we obtain the following equations for $F^{(1)}(E_h(\mathbf{k}),I)$ and $G^{(1)}(E_l(\mathbf{k}),I)$ for states in the resonant region:

$$F^{(1)}(E_h(\mathbf{k}),I)=\sum_{\mathbf{k}'} R^{(\text{elastic})}_{h\mathbf{k}'\to h\mathbf{k}}\left[\frac{-\beta(\mathbf{k}',I)T_h(\mathbf{k})[f_h^e(\mathbf{k})-f_l^e(\mathbf{k}')]}{1+\beta(\mathbf{k}',I)[T_h(\mathbf{k})+T_l(\mathbf{k}')]}+\frac{T_h(\mathbf{k})+\beta(\mathbf{k}',I)T_h(\mathbf{k})T_l(\mathbf{k}')}{1+\beta(\mathbf{k}',I)[T_h(\mathbf{k})+T_l(\mathbf{k}')]}F^{(0)}(E_h(\mathbf{k}'),I)\right.$$
$$\left.+\frac{\beta(\mathbf{k}',I)T_h(\mathbf{k})T_l(\mathbf{k}')}{1+\beta(\mathbf{k}',I)[T_h(\mathbf{k})+T_l(\mathbf{k}')]}G^{(0)}(E_l(\mathbf{k}'),I)+T_h(\mathbf{k})G^{(0)}(E_h(\mathbf{k}'),I)\right] \tag{A6}$$

and

$$G^{(1)}(E_l(\mathbf{k}),I)=\sum_{\mathbf{k}'} R^{(\text{elastic})}_{l\mathbf{k}'\to l\mathbf{k}}\left[\frac{\beta(\mathbf{k}',I)T_l(\mathbf{k})[f_h^e(\mathbf{k}')-f_l^e(\mathbf{k})]}{1+\beta(\mathbf{k}',I)[T_h(\mathbf{k}')+T_l(\mathbf{k})]}+\frac{T_l(\mathbf{k})+\beta(\mathbf{k}',I)T_h(\mathbf{k}')T_l(\mathbf{k})}{1+\beta(\mathbf{k}',I)[T_h(\mathbf{k}')+T_l(\mathbf{k})]}G^{(0)}(E_l(\mathbf{k}'),I)\right.$$
$$\left.+\frac{\beta(\mathbf{k}',I)T_h(\mathbf{k}')T_l(\mathbf{k})}{1+\beta(\mathbf{k}',I)[T_h(\mathbf{k}')+T_l(\mathbf{k})]}F^{(0)}(E_h(\mathbf{k}'),I)+T_l(\mathbf{k})F^{(0)}(E_l(\mathbf{k}'),I)\right]. \tag{A7}$$

The terms in $F^{(1)}$ and $G^{(1)}$ associated with the first-order corrections, $f_h^{(1)}-f_h^{(0)}$ and $f_l^{(1)}-f_l^{(0)}$, are found to be much smaller than the terms in $F^{(1)}$ and $G^{(1)}$ associated with the zeroth-order approximation to $f_h^{(0)}$ and $f_l^{(0)}$. We use the first-order expressions for $F^{(1)}(E_h(\mathbf{k}),I)$ and $G^{(1)}(E_l(\mathbf{k}),I)$ to calculate the second-order approximations to f_h and f_l. These higher-order expressions for $f_h(\mathbf{k},I)$ and $f_l(\mathbf{k},I)$ are then substituted into the definitions for F and G to obtain

$$F^{(2)}(E_h(\mathbf{k}),I)=\sum_{\mathbf{k}'} R^{(\text{elastic})}_{h\mathbf{k}'\to h\mathbf{k}}\left[\frac{-\beta(\mathbf{k}',I)T_h(\mathbf{k})[f_h^e(\mathbf{k})-f_l^e(\mathbf{k}')]}{1+\beta(\mathbf{k}',I)[T_h(\mathbf{k})+T_l(\mathbf{k}')]}+\frac{T_h(\mathbf{k})+\beta(\mathbf{k}',I)T_h(\mathbf{k})T_l(\mathbf{k}')}{1+\beta(\mathbf{k}',I)[T_h(\mathbf{k})+T_l(\mathbf{k}')]}F^{(1)}(E_h(\mathbf{k}'),I)\right.$$
$$\left.+\frac{\beta(\mathbf{k}',I)T_h(\mathbf{k})T_l(\mathbf{k}')}{1+\beta(\mathbf{k}',I)[T_h(\mathbf{k})+T_l(\mathbf{k}')]}G^{(1)}(E_l(\mathbf{k}'),I)+T_h(\mathbf{k})G^{(1)}(E_h(\mathbf{k}'),I)\right] \tag{A8}$$

and

$$G^{(2)}(E_l(\mathbf{k}),I)=\sum_{\mathbf{k}'} R^{(\text{elastic})}_{l\mathbf{k}'\to l\mathbf{k}}\left[\frac{\beta(\mathbf{k}',I)T_l(\mathbf{k})[f_h^e(\mathbf{k}')-f_l^e(\mathbf{k})]}{1+\beta(\mathbf{k}',I)[T_h(\mathbf{k}')+T_l(\mathbf{k})]}+\frac{T_l(\mathbf{k})+\beta(\mathbf{k}',I)T_h(\mathbf{k}')T_l(\mathbf{k})}{1+\beta(\mathbf{k}',I)[T_h(\mathbf{k}')+T_l(\mathbf{k})]}G^{(1)}(E_l(\mathbf{k}'),I)\right.$$
$$\left.+\frac{\beta(\mathbf{k}',I)T_h(\mathbf{k}')T_l(\mathbf{k})}{1+\beta(\mathbf{k}',I)[T_h(\mathbf{k}')+T_l(\mathbf{k})]}F^{(1)}(E_h(\mathbf{k}'),I)+T_l(\mathbf{k})F^{(1)}(E_l(\mathbf{k}'),I)\right]. \tag{A9}$$

The terms associated with the second-order corrections, $f_l^{(2)}(\mathbf{k},I)-f_l^{(1)}(\mathbf{k},I)$, are also much smaller than the terms associated with the first-order corrections. We truncate the expansion for $F(\mathbf{k},I)$ and $G(\mathbf{k},I)$ to second order in $f_h(\mathbf{k},I)$ and $f_l(\mathbf{k},I)$ and use Eqs. (A8) and (A9) to obtain approximate values for the modified feeding rate of holes into resonant states of the heavy- and light-hole bands.

[1]G. W. Gobeli and H. Y. Fan, Phys. Rev. **119**, 613 (1960).
[2]R. Braunstein, J. Phys. Chem. Solids **8**, 280 (1959).
[3]A. H. Kahn, Phys. Rev. **97**, 1647 (1955).
[4]J. W. Hodby, Proc. Phys. Soc. London **82**, 324 (1963).
[5]W. M. Becker, A. K. Ramdas, and H. Y. Fan, J. Appl. Phys. **32**, 2094 (1961).
[6]F. Matossi and F. Stern, Phys. Rev. **111**, 472 (1958).
[7]C. R. Phipps, Jr. and S. J. Thomas, Opt. Lett. **1**, 93 (1977).
[8]R. L. Carlson, M. D. Montgomery, J. S. Ladish, and C. M. Lockhart, IEEE J. Quantum Electron. **QE-13**, 35 (1977).
[9]F. Keilmann, IEEE J. Quantum Electron. **QE-12**, 592 (1976).
[10]R. B. James, E. Schweig, D. L. Smith, and T. C. McGill, Appl. Phys. Lett. **40**, 231 (1982).
[11]M. Kawai and T. Miyakawa, Jpn. J. Appl. Phys. **20**, 369 (1981).
[12]A. F. Gibson, C. A. Rosito, C. A. Raffo, and M. F. Kimmitt, Appl. Phys. Lett. **21**, 356 (1972).
[13]R. B. James, W. H. Christie, R. E. Eby, B. E. Mills, and L. S. Darken, Jr., J. Appl. Phys. **59**, 1323 (1986).
[14]B. J. Feldman and J. F. Figueria, Appl. Phys. Lett. **25**, 301 (1974).
[15]A. F. Gibson, M. F. Kimmitt, and B. Norris, Appl. Phys. Lett. **24**, 306 (1974).
[16]A. J. Alcock and A. C. Walker, Appl. Phys. Lett. **25**, 299 (1974).
[17]M. Sargent III, Opt. Commun. **20**, 298 (1977).
[18]R. B. James and D. L. Smith, Phys. Rev. Lett. **42**, 1495 (1979).
[19]R. B. James and D. L. Smith, Phys. Rev. B **21**, 3502 (1980).
[20]C. K. N. Patel, P. Fleury, R. Slusher, and H. Frisch, Phys. Rev. Lett. **16**, 971 (1966).
[21]R. E. Slusher, W. Giriat, and S. R. J. Brueck, Phys. Rev. **183**, 758 (1969).
[22]A. M. Danishevskii, A. A. Patrin, S. M. Ryvkin, and I. D. Yaroshetskii, Zh. Eksp. Teor. Fiz. **56**, 1457 (1969) [Sov. Phys.—JETP **29**, 781 (1969)].
[23]H. J. Fossum and B. Ancker-Johnson, Phys. Rev. B **8**, 2850 (1973).
[24]H. J. Fossum, W. S. Chen, and B. Ancker-Johnson, Phys. Rev. B **8**, 2857 (1973).
[25]H. J. Fossum and D. B. Chang, Phys. Rev. B **8**, 2842 (1973).
[26]C. C. Lee and H. Y. Fan, Phys. Rev. B **9**, 3502 (1974).
[27]J. M. Doviak, A. F. Gibson, M. F. Kimmitt, and A. C. Walker, J. Phys. C **6**, 593 (1973).
[28]A. F. Gibson, C. B. Hatch, P. N. D. Maggs, D. R. Tilley, and A. C. Walker, J. Phys. C **9**, 3259 (1976).
[29]T. Grave, E. Scholl, and H. Wurz, J. Phys. C **16**, 1693 (1983).
[30]S. A. Jamison and A. V. Nurmikko, Phys. Rev. B **19**, 5185 (1979).
[31]B. D. Schwartz, P. M. Fauchet, and A. V. Nurmikko, Opt. Lett. **5**, 371 (1980).
[32]E. O. Kane, J. Phys. Chem. Solids **1**, 82 (1956).
[33]P. Lawaetz, Phys. Rev. B **4**, 3460 (1971).
[34]S. W. Kurnick and J. M. Powell, Phys. Rev. **116**, 597 (1959).
[35]R. B. James and D. L. Smith, IEEE J. Quantum Electron. **QE-18**, 1841 (1982).
[36]E. M. Conwell, *High Field Transport in Semiconductors* (Academic, New York, 1967).
[37]J. D. Wiley and M. DiDomenico, Jr., Phys. Rev. B **2**, 427 (1970).
[38]D. M. Brown and R. Bray, Phys. Rev. **127**, 1593 (1962).
[39]R. B. James and D. L. Smith, J. Appl. Phys. **51**, 2836 (1980).
[40]H. Brooks, in *Advances in Electronics and Electron Physics*, edited by L. Marton (Academic, New York, 1955), Vol. 7, p. 85.
[41]I. N. Yassievich and I. D. Yaroshetskii, Fiz. Tekh. Poluprovodn. **9**, 57 (1975) [Sov. Phys.—Semicond. **9**, 565 (1975)].
[42]See, for example, A. L. Smirl, T. F. Boggess, B. S. Wherrett, G. P. Perryman, and A. Miller, IEEE J. Quantum Electron. **QE-19**, 690 (1983).
[43]A. M. Johnston, C. R. Pidgeon, and J. Dempsey, Phys. Rev. B **22**, 825 (1980).
[44]A. K. Kar, J. G. H. Mathew, S. D. Smith, B. Davis, and W. Prettl, Appl. Phys. Lett. **42**, 334 (1983).
[45]T. Elsaesser, H. Lobentanzer, and W. Kaiser, Appl. Phys. Lett. **47**, 1190 (1985).
[46]P. Mukherjee, M. Shiek-bahaei, and H. S. Kwok, Appl. Phys. Lett. **46**, 770 (1985).
[47]J. G. H. Mathew, A. K. Kar, N. R. Heckenberg, and I. Galbraith, IEEE J. Quantum Electron. **QE-21**, 94 (1985).
[48]M. Sheik-bahaei, P. Mukherjee, and H. S. Kwok, J. Opt. Soc. Am. B **3**, 379 (1986).
[49]W. Ji, A. K. Kar, P. L. Chua, and A. C. Walker, IEEE J. Quantum Electron. **QE-23**, 1986 (1987).